Journal of Microscopy, 2010
Received 12 October 2009; accepted 7 January 2010
doi: 10.1111/j.1365-2818.2010.03369.x

Confined displacement algorithm determines true and random colocalization in fluorescence microscopy

O. RAMÍREZ*,†,§, A. GARCÍA*, R. ROJAS*,‡, A. COUVE†,§ & S. HÄRTEL*,§
*Laboratory for Scientific Image Analysis (SCIAN-Lab) at the Anatomy and Developmental Biology Program, ICBM, Universidad de Chile, Santiago, Chile
†Program of Physiology and Biophysics, ICBM, Universidad de Chile, Santiago, Chile
‡Xperts Ldta, Valdivia, Valparaíso, Santiago, Chile
§Nucleus of Neural Morphogenesis NEMO, ICBM, Faculty of Medicine, Universidad de Chile, Santiago, Chile

Key words. Confined cellular compartments, image correlation spectroscopy, Manders colocalization coefficients, probability density function, random scenario.

Summary

The quantification of colocalizing signals in multichannel fluorescence microscopy images depends on the reliable segmentation of corresponding regions of interest, on the selection of appropriate colocalization coefficients, and on a robust statistical criterion to discriminate true from random colocalization. Here, we introduce a confined displacement algorithm based on image correlation spectroscopy in combination with Manders colocalization coefficients $M1_{ROI}$ and $M2_{ROI}$ to quantify true and random colocalization of a given florescence pattern. We show that existing algorithms based on block scrambling exaggerate the randomization of fluorescent patterns with resulting inappropriately narrow probability density functions and false significance of true colocalization in terms of p values. We further confine our approach to subcellular compartments and show that true and random colocalization can be analysed for model dendrites and for $GABA_B$ receptor subunits $GABA_BR1/2$ in cultured hippocampal neurons. Together, we demonstrate that the confined displacement algorithm detects true colocalization of specific fluorescence patterns down to subcellular levels.

Introduction

The term colocalization refers to the presence of different molecules, organelles, cells or tissue at the same physical location. Different techniques have been used to address the question of relative proximities within their physical resolution limits, for example co-immunoprecipitation, fluorescence resonance energy transfer (David *et al.*, 2007), single molecule colocalization imaging (Koyama-Honda *et al.*, 2005), fluorescence lifetime imaging microscopy (Berezovska *et al.*, 2003), fluorescence correlation or cross-correlation spectroscopy (Bacia & Schwille, 2007) and spatial image cross-correlation spectroscopy (Comeau *et al.*, 2006). However, most colocalization studies rely on two-channel fluorescence imaging techniques that localize cellular constituents with high specificity and sensitivity (Hell *et al.*, 2004; Betzig *et al.*, 2006; Bolte & Cordelieres, 2006; Schermelleh *et al.*, 2008).

The advantages and pitfalls of existing approaches to quantify colocalization are still a matter of debate. Even the widely used Pearson's correlation coefficient provokes considerable controversy, emphasizing the current need to develop common criteria for the evaluation of colocalization (Bolte & Cordelieres, 2006; Comeau *et al.*, 2006; Adler & Parmryd, 2007; Bolte, 2007; Adler *et al.*, 2008). An increasing number of investigators opt for Manders colocalization coefficients $M1/2$, which determine the ratio between colocalizing to non-colocalizing signals in a channel-specific manner (Manders *et al.*, 1993; Costes *et al.*, 2004; Comeau *et al.*, 2006; Vidal *et al.*, 2007; Comeau *et al.*, 2008; Parra *et al.*, 2008; Sanchez *et al.*, 2008; Savio-Galimberti *et al.*, 2008; Espinosa *et al.*, 2009; Ramirez *et al.*, 2009). Current controversies can be summarized by three basic issues: (1) should segmentation of regions of interests (ROIs) be subjected to automated or subjective criteria (Lachmanovich *et al.*, 2003; Costes *et al.*, 2004; Bolte & Cordelieres, 2006), (2) which coefficient yields the best estimate for colocalization (Manders *et al.*, 1992, 1993; Costes *et al.*, 2004; Comeau *et al.*, 2006) and (3) does the selected coefficient characterize a

Correspondence to: Steffen Härtel, Laboratory for Scientific Image Analysis, ICBM, Facultad de Medicina, Universidad de Chile, Independencia 1027, Santiago, Chile. Tel: +56-2-978-6366; fax: +56-2-978-6368; e-mail: shartel@med.uchile.cl

statistically significant scenario (Lachmanovich *et al.*, 2003; Costes *et al.*, 2004; Comeau *et al.*, 2008)? These issues were recently addressed with a proposed automated method for segmentation, the calculation of modified Manders coefficients $M1/2_{\mathrm{Auto}}$ and a statistical validation of colocalization in terms of p values by a combination of block scrambling, calculation of PC values, and probability density functions (PDFs) (Costes *et al.*, 2004). Despite the undisputed merit of this approach, the authors outlined a number of pitfalls and limitations that still remained. Further discussion followed (Bolte & Cordelieres, 2006), and alternative techniques based on ICCS were promoted (e.g. Comeau *et al.*, 2006) to overcome the limitations of Costes' approach for scenarios with high and asymmetric signal densities. ICCS calculates modified Manders coefficients $M1/2_{\mathrm{ICCS}}$ from auto- and cross-correlation functions in combination with Gaussian fits of the respective zero lag amplitudes. Statistical significance for $M1/2_{\mathrm{ICCS}}$ is defined by *ad hoc* criteria, leading to a detection limit of ~20% (Comeau *et al.*, 2006), compared to ~3% reported for Costes' block scrambling (Costes *et al.*, 2004). Recently, parallel two-channel block scrambling with a block size of ~400 nm was incorporated into the ICCS approach resulting in an improved robustness of the fitting procedure (Comeau *et al.*, 2008). Previously, a block dimension of the full width at half maximum (FWHM) value of the microscopic point spread function (PSF) of ~200 nm had been suggested (Costes *et al.*, 2004). Both algorithms alter the visual perception of the subjacent fluorescent pattern severely, and no data has been published so far that proves block scrambling as a reliable random scenario for significance tests of colocalization.

In this paper, we present an approach that overcomes the limitations of previously published methods. The development of our approach was driven by the observation that different experimental systems in our laboratory could not be analysed satisfactorily with existing methods (Vidal *et al.*, 2007; Sanchez *et al.*, 2008; Parra *et al.*, 2008; Espinosa *et al.*, 2009; Ramirez *et al.*, 2009). In particular, we were increasingly concerned about (1) unsatisfactory results for automated segmentation (Costes *et al.*, 2004), (2) uncertainties regarding the quality of random scenarios generated by block scrambling and (3) quantifying colocalization in dendrites and small subcellular compartments, which have been considered to be inaccessible until today (Comeau *et al.*, 2008). To validate our approach, we generated model images with defined degrees of colocalizing point signals. Specifically, we mimicked fluorescent patterns for $GABA_B$ receptor subunits $GABA_BR1$ and $GABA_BR2$ in dendrites of hippocampal neurons. We demonstrated that Laplace filters lead to reliable results for the segmentation of point signals in model systems and hippocampal neurons. We also introduced modified Manders coefficients $M1/2_{\mathrm{ROI}}$ in combination with image correlation techniques to access true and random colocalization on a statistical level. We further confine our approach to selected compartments, an essential step in performing statistically valid colocalization analysis at a subcellular level.

Our approach, coined confined displacement algorithm (CDA), can be understood as a modification of ICCS (Comeau *et al.*, 2006, 2008) or of the dual channel cross-correlation approach (Barbarese *et al.*, 1995). Alternatively, it can be regarded as a two-dimensional extension of Van Steensel's method, who calculated PC values along displacements in the x-axis (van Steensel *et al.*, 1996). We here apply the CDA in combination with PC and $M1/2_{\mathrm{ROI}}$ values, generate PDFs for random scenarios and then compare the results to block scrambling. We show that block scrambling, but not CDA, leads to over-randomization and carries the risk of producing false-positive colocalization results. Finally, we show how confining colocalization analysis to specific compartments generates realistic random scenarios within biological structures and demonstrate the potential to quantify colocalization of $GABA_BR1/R2$ in neuronal dendrites, the region near the plasma membrane (PM), and the core region of the dendrites. We have elsewhere reported on the practical application of CDA for a detailed analysis of the assembly of heteromeric $GABA_B$ subunits in dendrites of hippocampal neurons (Ramirez *et al.*, 2009).

Materials and methods

Neuronal cultures and transfection

Adult pregnant female Sprague-Dawley E18 rats were purchased from the Universidad Católica de Chile and killed in CO_2 chambers according to the Guide for Care and Use of Laboratory Animals (1996, National Academy of Sciences). Primary hippocampal neurons were cultured and transfected by Ca^{2+} phosphate as described (Banker & Goslin, 1988), and analysed 48–72 h posttransfection.

DNA constructs, antibodies and immunofluorescence

MYC-$GABA_BR1$ and HA-$GABA_BR2$ have been described (Couve *et al.*, 1998). MYC antibodies from Sigma (St. Louis, MI), and influenza A Virus epitope (HA) antibodies from Roche (Indianapolis, IN). Chicken $GABA_BR1$ antibody (which recognizes $GABA_BR1a$ and $GABA_BR1b$) against intracellular C-terminal domain was provided by S.J. Moss (Tufts University, MA). Guinea pig $GABA_BR2$ was purchased from Chemicon (Temecula, CA). Secondary anti-mouse, anti-rabbit, anti-guinea pig or anti-chicken antibodies conjugated to Texas Red (TR), tetramethyl rhodamine isothiocyanate (TRITC) or fluorescein isothiocyanate (FITC) were purchased from Jackson Research Laboratories (West Grove, PA). Immunofluorescence was performed as previously described (Vidal *et al.*, 2007).

Confocal microscopy and deconvolution

Confocal laser scanning microscopy was performed with a Zeiss LSM-5, Pascal 5 Axiovert 200 microscope, using LSM 5 3.2 software and a 63×/1.4 Oil DIC objective. Image stacks were recorded in multitrack mode with intensity $I(x,y,z) \in [0,255]$, and voxel size $\Delta x/\Delta y/\Delta z = 70/70/300$ nm. Ch-1 for FITC: $\lambda_{exc}/\lambda_{em} = 488/505 - 530$ nm. Ch-2 for TR/TRITC: $\lambda_{exc}/\lambda_{em} = 543/>560$ nm. We guaranteed that $I(x,y,z)$ did not saturate and that image background was slightly above zero. A spatial shift in the focal *xy*-plane was calibrated with a grid and corrected for all images. Image stacks were deconvolved with Huygens Scripting Software (SVI, Hilversum, The Netherlands) using the Classic Maximum Likelihood Estimator. The signal-to-noise ratio was adjusted until the deconvolved images were free of pixel noise. We restricted colocalization analysis to *xy*-planes as most imaging techniques such as confocal laser scanning microscopy, spinning disk, two-photon or conventional fluorescence microscopy yield PSFs which are at least elongated by a factor of 2.5 in the *z*-axis.

Image processing and statistical analysis

We developed image-processing routines with interactive data language (ITT, Boulder, CO), for the generation of synthetic image series with defined degrees of colocalization and convolution with channel-specific PSFs, the segmentation of ROIs, colour visualization, calculation of PC or $M1/2_{ROI}$ and for the statistical validation of PCs and $M1/2_{ROI}$ by the CDA based on PDFs. For the statistical validation in Fig. 4b, we used OriginPro 7.0 (OriginLab Corp., Northampton, MA).

Model dendrites with defined degrees of colocalization

Model dendrites with defined degrees of colocalization were generated in 128 × 128 pixel frames. PSFs and Nyquist distances were calculated (http://support.svi.nl/wiki/NyquistCalculator) for a pixel size slightly below the Nyquist distance (40 nm). The diameter of 2.44 μm represents a mean dendrite diameter determined from $N = 10$ hippocampal neurons. One hundred and twenty point signals with $I = 50$ were seeded inside the area of the model dendrite ($I = 1$) using the Box–Muller transform for uniformly distributed random numbers (Box & Muller, 1958). The percentage of colocalization was calculated by $N \times 100/120$, where $N = [0–120]$ is the number of colocalizing point sources. The sum of dendrite and point signal image was convolved with channel-specific PSFs to mimic fluorescence pattern of $GABA_BR1/R2$ signals.

Segmentation of ROIs

We applied isotropic Laplace filters with a radius $r = 4$ for segmentation of signals in model dendrites and $GABA_BR1/R2$ signals in hippocampal neurons. This operation presents a convolution of the original image $I(x,y)$ with a kernel k: $k[x,y] \otimes I[x,y] = I'[x,y]$ (Fig. S1A). After convolution, selected thresholds values $I'[x,y]$ define the corresponding ROIs. Segmentation of dendrite shafts in model dendrites and neuronal projections was obtained by intensity thresholds. Morphologic filters filled remaining holes and removed signals outside the neuronal projections. Active contour models (Härtel *et al.*, 2007; Fanani *et al.*, 2009) were adjusted to the morphology of the borders. The quality of the segmentation was controlled by superposition of the original images over the ROIs. Segmentation of the PM was achieved by border-distance filters that were applied to the segmented dendrite shafts. The border-distance filter set each pixel inside an ROI to the closest border using Euclidean distance. Threshold values define a border thickness of 400 ± 40 nm, which include all fluorescent signals emitted from the PM in nonpermeabilized neurons transfected with MYC-$GABA_BR1$ and HA-$GABA_BR2$. Here, fluorescent signals were restricted to epitopes exposed towards the extracellular side of the PM. The core region in model dendrites was defined by subtracting the PM from the dendrite shaft. Segmentation methods were constant throughout experiments.

Colocalization based on $M1/2_{ROI}$ and PC, CDA, PDF, block scrambling and confinement to cellular compartments

For the quantification of channel-selective colocalization, we defined modified Manders colocalization coefficients $M1/2_{ROI}$ in previously segmented ROIs:

$$M1_{ROI} = \frac{\sum_{ij} I_{Ch1(ROI1(x_i,y_j) \cap ROI2(x_i,y_j))}}{\sum_{ij} I_{Ch1(ROI1(x_i,y_j))}},$$
$$M2_{ROI} = \frac{\sum_{ij} I_{Ch2(ROI1(x_i,y_j) \cap ROI2(x_i,y_j))}}{\sum_{ij} I_{Ch2(ROI2(x_i,y_j))}} \quad (1)$$

$I_{Ch1}(ROI1(x_i,y_j) \cap ROI2(x_i,y_j))$ and $I_{Ch2}(ROI1(x_i,y_j) \cap ROI2(x_i,y_j))$ sum up the fluorescent intensities inside the colocalizing regions, $I_{Ch1}(ROI1(x_i,y_j))$ and $I_{Ch2}(ROI2(x_i,y_j))$ sum up the fluorescent intensities inside the respective ROIs across the image matrix. Thereby, $M1/2_{ROI} \in [0,1]$ quantify the amount of colocalizing fluorescence in respect to the total amount of fluorescent signals in each respective ROI.

To obtain random scenarios, we implemented image correlation techniques, which shift one channel and its corresponding image mask relative to the second channel. This two-dimensional image correlation technique calculates $M1_{ROI}(d)$, $M2_{ROI}(d)$ or $PC(d)$ as a function of radial

displacements d:

$$M1_{\mathrm{ROI}}(d) = M1_{\mathrm{ROI}}(x', y'|\sqrt{x'^2 + y'^2} = d) = \frac{\sum_{ij} I_{\mathrm{Ch1(ROI1}(x_i,y_j)\cap \mathrm{ROI2}(x_i+x', y_j+y'))}}{\sum_{ij} I_{\mathrm{Ch1(ROI1}(x_i,y_j))}} \quad (2)$$

$$M2_{\mathrm{ROI}}(d) = M2_{\mathrm{ROI}}(x', y'|\sqrt{x'^2 + y'^2} = d) = \frac{\sum_{ij} I_{\mathrm{Ch2(ROI1}(x_i,y_j)\cap \mathrm{ROI2}(x_i+x', y_j+y'))}}{\sum_{ij} I_{\mathrm{Ch2(ROI2}(x_i+x', y_j+y'))}} \quad (3)$$

$$\mathrm{PC}(d) = \mathrm{PC}\left(x', y'|\sqrt{x'^2 + y'^2} = d\right) = \frac{\sum_{ij}\left(I_{\mathrm{Ch1}(x_i,y_j)} - \bar{I}_{\mathrm{Ch1}}\right)\left(I_{\mathrm{Ch2}(x_i+x', y_j+y')} - \bar{I}_{\mathrm{Ch2}}\right)}{\sqrt{\sum_{ij}\left(I_{\mathrm{Ch1}(x_i,y_j)} - \bar{I}_{\mathrm{Ch1}}\right)^2 \sum_{ij}\left(I_{Ch2(x_i+x', y_j+y')} - \bar{I}_{\mathrm{Ch2}}\right)^2}} \quad (4)$$

For a maximum displacement d', pixel shifts are applied for all x' and y' within $\sqrt{x'^2 + y'^2} \leq d'$: $x' \in [-d', d']$, $y' \in [-d', d']$. For each shift $[x', y']$, one data value is obtained as a function of the Euclidian distance $d = \sqrt{x'^2 + y'^2}$. Successive shifts lead to one value for $d = 0$, four values for $d = 1$, $d = \sqrt{2}$ and $d = 2$, eight values for $d = \sqrt{5}$, etc. For the data presented in Figs. 3 and 5, we rounded the d values to the closest integer and calculated mean and SD values for each respective distance. The ImageJ and online version of the implementation of Eqs. 2 and 3 plot $M1/2_{\mathrm{ROI}}$ as a function of d values without rounding and offers the possibility to download an ASCII list of distance d, $M1_{\mathrm{ROI}}(d)$ and $M2_{\mathrm{ROI}}(d)$ (www.scian.cl). By contrast to $M1/2_{\mathrm{ROI}}(d)$, PC(d) does not depend on ROIs. $\bar{I}_{\mathrm{Ch1}}$ and $\bar{I}_{\mathrm{Ch2}}$ are the average intensities in the respective channels (Eq. 4).

With increasing d, $M1/2_{\mathrm{ROI}}(d)$ and PC(d) approach values that represent random scenarios for a given signal distribution. From these random values, PDFs can be calculated to test if the colocalization coefficients that were calculated at the original image position [$M1/2_{\mathrm{ROI}}(d = 0)$ or PC($d = 0$)] are statistically different from a random population in terms of p values.

The CDA can only lead to a reliable characterization of random colocalization if the subjacent fluorescence patterns are nonperiodic and isotropically distributed inside an image frame. However, this is not the case for most biological structures. We therefore developed an algorithm which confines radial displacements to previously defined cellular compartments. Thereby, pixels that are shifted out of these compartments replace missing pixels at the opposite side: signal density, mean signal intensity and signal pattern are maintained, and CDA plots reliably represent random scenarios. Example movies that show the complete analysis of the CDA in model dendrites, hippocampal neurons the core region, and the PM are available in 'Supporting Information'. To compare the performance of the CDA to previously applied randomization algorithms, we implemented block scrambling (Costes *et al.*, 2004). For block scrambling, one image channel and its corresponding image mask were divided into independent blocks of pixel size $n \times n$. These blocks were scrambled synchronically, and $M1/2_{\mathrm{ROI}}$ or PC values were calculated. We compared different block sizes and applied 500 consecutive iterations to calculate PDFs for each respective random scenario.

Results

Fluorescent point sources in model dendrites and cultured hippocampal neurons

In cultured hippocampal neurons, $GABA_BR1/R2$ show regular fluorescent pattern of densely packed granules independent of the dendrite diameter (Fig. 1a). The importance of deconvolution for structures below or at the limit of resolution is outlined in Fig. 1b. Deconvolved images are free of photon noise and signals can be clearly distinguished. Because deconvolution removes photon noise, we do not discuss its implication for colocalization analysis in this work. The fidelity of the fluorescent pattern observed for $GABA_BR1/R2$ after deconvolution can be tested by successive acquisition of the same dendrite section with slightly shifted microscopic *xyz*-positions. Because these controls modify the input data for the deconvolution algorithm, the results only lead to identical fluorescent pattern when the algorithm is robust. This was the case for all presented experiments.

Figure 2 shows model dendrites with diffraction limited point sources that mimic the fluorescent $GABA_BR1/R2$ signals of the primary dendrites shown in Fig. 1. After convolution with the channel-selective PSFs, intensity and morphological patterns with respect to size, shape and density of the point signals were found to be very similar to those of the neuronal system. Intensity line scans across model and neuronal dendrites had a high degree of similarity (not shown). ROIs in the model dendrites cover 28.9%/30.9% (Fig. 2b, bottom) and 28.9%/34.1% of the neuronal dendrites (Fig. 1b, bottom). The FWHM values of the PSFs used for the convolution of the model dendrites differ by ~11% (181/205 nm; Fig. 2a, bottom right). Convolution of identical initial models with different PSFs produced scatter plots that deviated from ideal behaviour (Fig. S1F). The broader PSF for the red channel leads to higher intensities and slightly different results for segmentation of the signal patterns when compared to the green channel (see 100% colocalization; Fig. 2b, bottom).

Validation of true versus random colocalization by the CDA

Figure 3a presents examples for block scrambling and the CDA for a displacement $d = 11$ in model dendrites with 100% colocalization. Scrambling with pixel blocks 1×1, 5×5 or 9×9 compromises the morphology of the

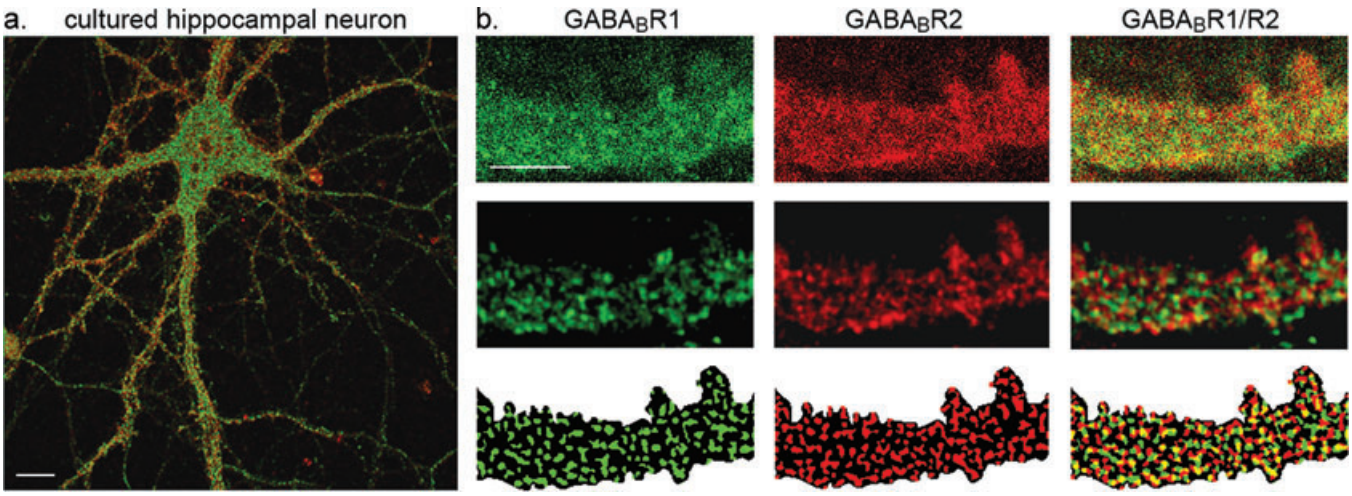

Fig. 1. (a) Confocal image of a cultured hippocampal neuron after deconvolution: GABA$_B$R1 (*green*), GABA$_B$R2 (*red*) and GABA$_B$R1/R2 (*yellow*). Scale bar represents 10 μm. (b) Detail of hippocampal dendrite before and after deconvolution (*top* and *center row*). *Bottom row* shows ROIs for dendrites (*black*), for GABA$_B$R1/R2 (*green*/*red*) and for colocalization signals (*yellow*) after segmentation. Scale bar represents 5 μm.

fluorescent pattern severely (Fig. 3a, I–III). By contrast, CDA at a radial displacement $d = 11$ produces a visual impression, which is similar to 0% colocalization (Fig. 3a, IV and VI). Figure 3b presents two plots with the most important characteristics for colocalization coefficients $M1_{ROI}$ (*left*) and PC (*right*) calculated as a function of radial displacements. Both CDA plots distinguish three regimes: (1) initial colocalization ($d = 0$), (2) successive randomization with increasing radial displacements ($d \geq 1$) and (3) random values when d exceeds the size of the segmented fluorescent signals d_S ($d \geq d_S$). For model dendrites with 0% colocalization, $M1_{ROI}$ and PC remain at the basal random level: $M1_{ROI} = 0.28$ and PC = 0 (*open squares*). For 50% and 100% colocalization, $M1_{ROI}$ and PC drop from the initial values at $d = 0$ (for

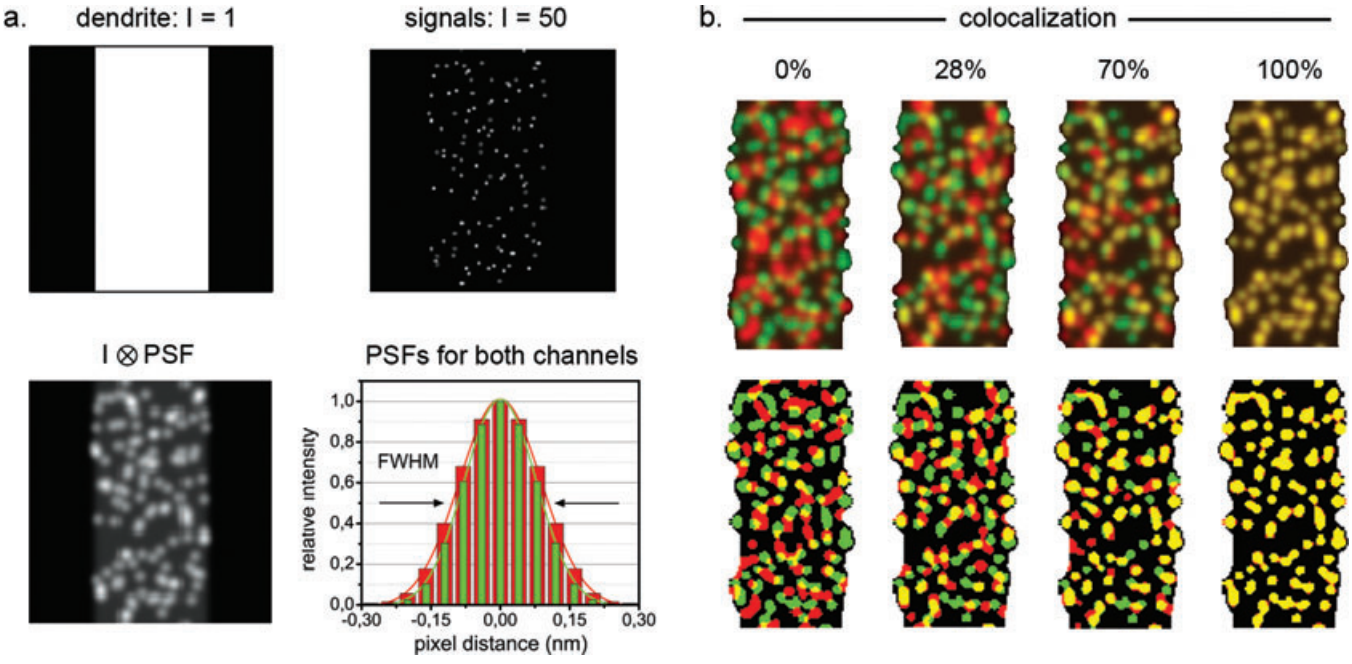

Fig. 2. Model dendrites mimic GABA$_B$R1/R2 signals in primary dendrites of hippocampal neurons. (a) The sum of the model dendrite (*top left*) and 120 point signals (*top right*) is convolved with the channel-specific PSF (*bottom row*). Arrows indicate the FWHM values of the PSFs calculated for GABA$_B$R1/R2 channels (Costes *et al.*, 2004). See 'Materials and methods' section for detailed description. (b) Dendrite models with defined degrees of colocalization (*upper row*). *Bottom row* shows segmented dendrites (*black*), non-colocalizing GABA$_B$R1/R2 signals (*green*/*red*) and colocalization signals (*yellow*).

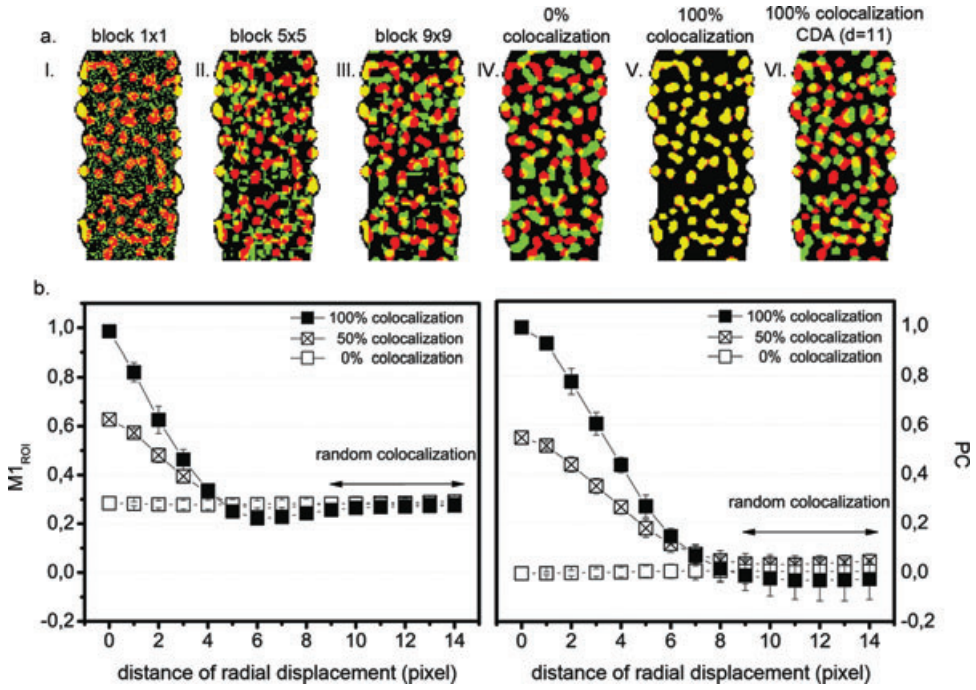

Fig. 3. CDA leads to random scenarios without compromising the subjacent fluorescence pattern. (a) Block scrambling for block sizes 1 × 1, 5 × 5 and 9 × 9 (*I–III*), dendrite models with 0% and 100% colocalization (*IV,V*), and CDA ($d = 11$) for 100% colocalization (*VI*). (b) CDA plots for $M1_{ROI}$ (*left*) and PC (*right*) in model dendrites with 0%, 50% and 100% colocalization (*black, crossed* and *open squares*). Mean values and corresponding SD are plotted for each distance. Arrows mark the random regime for colocalization in the asymptotic region of the plot ($9 \leq d \leq 14$).

50%: $M1_{ROI} = 0.63$ and PC = 0.55; for 100%: $M1_{ROI} = 0.99$ and PC = 0. 99) towards the basal random level at $d \geq 10$. An apparently high $M1_{ROI}$ value of 0.63 for 50% colocalization makes sense, if one considers that the $M1_{ROI}$ value for 100% yields 0.99 and random colocalization yields 0.28. In this case, the dynamic range for $M1_{ROI}$ values between 100% and random colocalization yields 0.99 – 0.28 = 0.71, and 50% of colocalization can be interpreted by the sum of the random value and half of the dynamic range 0.28 + 0.71/2 = 0.635, which fits perfectly well with the calculated $M1_{ROI}$ value of 0.63. The same rationale does not apply to the PC, where 0.55 is more than 5% higher than the expected value of 0.495. $M2_{ROI}$ values are similar to $M1_{ROI}$ values (not shown). In conclusion, CDAs lead to random scenarios without compromising the intrinsic fluorescence pattern and yield all the necessary information to test the statistical significance of true versus random colocalization.

From the random regime of the CDA plots for $M1_{ROI}(10 \leq d \leq 14)$, PC$(10 \leq d \leq 14)$, and the data derived from the block scrambling algorithms, PDFs were calculated which reflect the probability of obtaining certain colocalization coefficients under random conditions (Fig. 4a). PDFs and the distribution-specific 2σ values were calculated by Gauss fitting of PC and $M1_{ROI}$ probability distributions (Fig. S2). As Figs. 4a and b show, 2σ values increase for blocks 1 × 1 to 9 × 9 by a factor of 2–3. They further increase for the PDFs calculated from the CDA. 2σ values for block 5 × 5 are significantly different to the 2σ values derived by the CDA. Block 9 × 9 and CDA values are significantly different for PC, but not for $M1_{ROI}$ data ($N = 3$). $M2_{ROI}$ behaves similarly to $M1_{ROI}$ (not shown). In conclusion, the visual impression of over-randomization by block scrambling is supported by the analysis of the $2o'$ values of the respective PDFs.

Confinement of the CDA to cellular compartments

A statistical model based on case-sensitive random scenarios must consider the specific morphology of the cellular compartment. Figure 5a shows different morphologic scenarios and CDA plots for a model dendrite with 0% colocalization. For free signals inside the region near the PM (compare PM/free signals and *white squares* in CDA plot), $M1_{ROI}$ values decrease steadily with increasing radial displacements. A reliable random scenario cannot therefore be generated. By contrast, signals that are confined to the PM (*black squares*), initial $M1_{ROI}$ values at $M1_{ROI}(d = 0) = 0.225$ stabilize at $M1_{ROI}(d \geq 9) = 0.25$. For signals confined inside the core region (*circles*), $M1_{ROI}$ values oscillate around $M1_{ROI} = 0.3$ for all d. For this example, colocalization in the PM is slightly below, and colocalization in the core region slightly above the value of the entire dendrite $M1_{ROI} = 0.275$ (Fig. 5a, bottom).

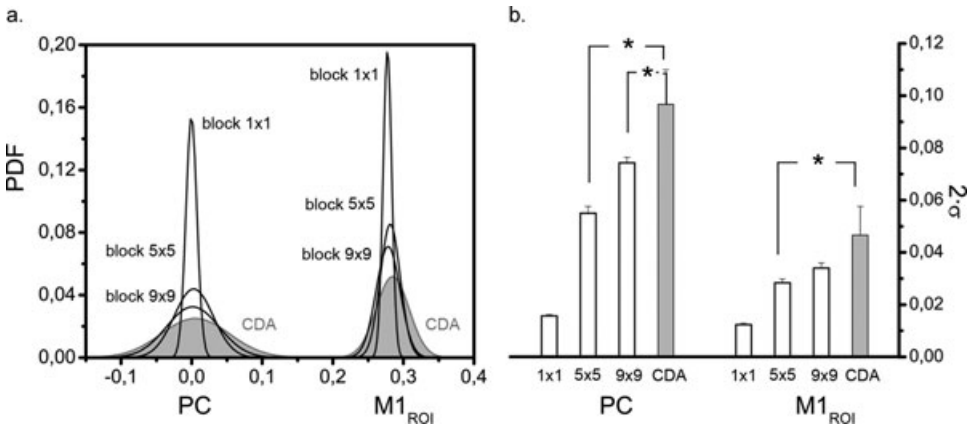

Fig. 4. (a) PDFs for PC and $M1_{ROI}$ were calculated from random values generated with block scrambling 1×1, 5×5, 9×9 and CDA (*light grey*) (compare to data shown in Fig. 3). Calculations were performed in 128×128 frames with 252 point sources and fluorescence patterns identical to the model dendrites (Fig. S3). Mean values from three different model scenarios were used to present the Gauss curves (see Fig. S2). (b) Mean values and SD of the 2σ values of the Gauss curves shown in (a) were calculated for PC and $M1_{ROI}$ for block 1×1, 5×5, 9×9 and CDA. *T*-test revealed statistical difference for PC (block 5×5 and CDA: $p < 0.006$ and block 9×9 and CDA: $p < 0.05$), and for $M1_{ROI}$ (block 5×5 and CDA: $p < 0.05$).

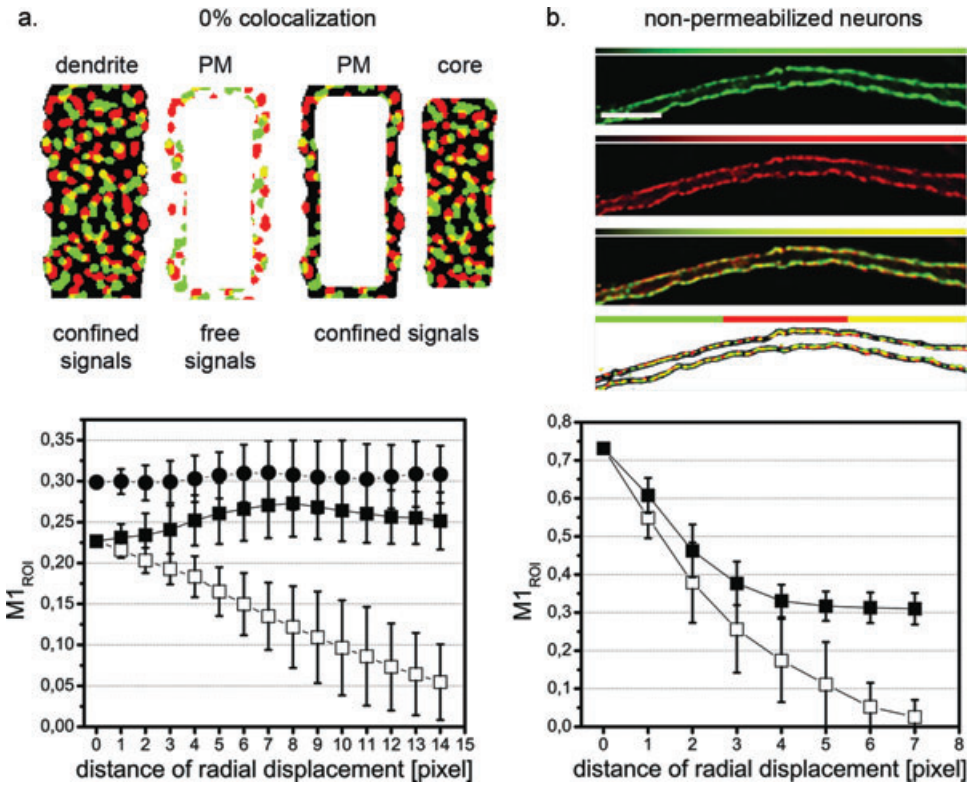

Fig. 5. CDA for free and confined signals in model dendrites with 0% colocalization and transfected neurons. (a) CDA for free signals inside the region near the plasma membrane (PM) (*white squares*), for signals confined to the PM (*black squares*) and for signals confined to the core region (*black circles*). (b) CDA for $GABA_BR1/R2$ signals inside the PM of a hippocampal neuron, cotransfected without permeabilization: MYC-$GABA_BR1$ (anti-MYC-FITC, *green*) and HA-$GABA_BR2$ (anti-HA-TRITC, *red*). The bottom image shows ROIs for $GABA_BR1/R2$ (*green*/*red*), colocalization (yellow) and the PM (*black*). CDA plot shows $M1_{ROI}$-values for free and confined signals (*white and black squares*). Scale bar represents 5 μm. CDA-plots show mean values and SD for each displacement.

CDA was tested in a subcellular compartment used as a positive control where complete colocalization of $GABA_BR1/R2$ is expected at the PM (Bettler *et al.*, 2004; Ramirez *et al.*, 2009). Our experimental approach yields staining of $GABA_BR1/R2$ subunits exclusively at the cell surface in both channels (Fig. 5b). We segmented a thin band of 400 ± 40 nm that contains all the PM subunits and defines a thin subcellular compartment amenable to CDA analysis. For free PM signals (*white squares*), $M1_{ROI}$ values drop in a similar manner as free PM signals of the model dendrite; a reliable conclusion for a random situation cannot be derived from this data. By contrast, CDA analysis for $M1_{ROI}$ confined to the PM shows a high and significant colocalization of $GABA_BR1/R2$ (*black squares*): $M1_{ROI}$ values drop asymptotically from ~ 0.73 at $d = 0$ to ~ 0.3 at $d > 5$.

Discussion

Automated versus qualitative/subjective segmentation

This paper focuses on an intuitive approach to quantifying true and random colocalization in cellular and subcellular compartments via standard confocal microscopy and computational image correlation techniques. Important pitfalls arising from improper sample preparation or microscopic acquisition have been discussed in detail before (Fink *et al.*, 1998; Landmann, 2002; Bolte & Cordelieres, 2006; Brown, 2007; Pearson, 2007; Scriven *et al.*, 2008). Recently, the importance of noise reduction prior to colocalization analysis has been emphasized (Adler *et al.*, 2008); to this end, sophisticated deconvolution software based on solid physical and probabilistic criteria should be preferred (Demandolx & Davoust, 1997; Lachmanovich *et al.*, 2003; Härtel *et al.*, 2007; Parra *et al.*, 2008; Espinosa *et al.*, 2009; Ramirez *et al.*, 2009). As we show for $GABA_BR1/R2$ signals in hippocampal neurons (Fig. 1b), deconvolution lowers Poisson noise to an imperceptible degree.

The selection of appropriate segmentation methods that define biological structures prior to colocalization analysis remains a controversial issue (Manders *et al.*, 1993; Lachmanovich *et al.*, 2003; Costes *et al.*, 2004; Bolte & Cordelieres, 2006; Comeau *et al.*, 2006, 2008). Although some authors prefer automated methods (Costes *et al.*, 2004), other authors advocate 'bias reduced' algorithms based on Sobel or Top Hat filters in combination with morphological operations (Lachmanovich *et al.*, 2003), or apply methods that are *per se* independent of segmentation procedures (Comeau *et al.*, 2006, 2008). For $GABA_BR1/R2$ signals in neuronal dendrites, reliable segmentation cannot be obtained with automated methods (Fig. S1). One possible reason for this is the proximity of point signals, which leads to overlapping intensities due to the extension of the PSFs. These pixels escape the 'anti-colocalization regions' of the bivariate histogram that is essential for the established stop criterion of the iterative segmentation algorithm (see Fig. 1 in Costes *et al.*, 2004). In addition, nonspecific antibody staining could also increase the background intensity level concomitantly inside the dendrite. Automated segmentation has been introduced for low and symmetric signal densities (Costes *et al.*, 2004), but it fails for medium to high signal densities, at colocalization above 60%, or for asymmetric scenarios (Comeau *et al.*, 2008). Unfortunately, most biological systems do not provide a combination of low, symmetric signal densities.

Manual setting of intensity thresholds lead to heterogeneous ROIs in respect to size, morphology and density across dendrites (Fig. S1). Instead, Laplace filters in combination with manual threshold settings provided a homogeneous segmentation pattern. We have observed that automated segmentation fails for fluorescence signals in cardiac tissue sections (Sanchez *et al.*, 2008), cultured cardiomyocytes (Parra *et al.*, 2008) or skeletal muscle cells (Espinosa *et al.*, 2009), but the application of mathematical filters and basic image-processing routines have produced satisfactory results.

Correlation and colocalization coefficients for true and random scenarios

Visual inspection of fluorescent channels can give a good estimation of colocalization when similarity is high (Fig. 2b). For intermediate and lower ranges, uncertainty increases and visual estimation leads to conflicting interrater judgments. To quantify colocalization more objectively, more than a dozen coefficients have been introduced, and new approaches are still emerging. We favour Manders coefficients (Manders *et al.*, 1993), which yield channel-specific information and are sensitive to experimental stimuli that change the fluorescence pattern of one structure independent of the other. In addition, $M1/2_{ROI}$ consider the total fluorescence inside segmented ROIs thus making them insensitive to fusion of point sources, which produce problems for region based 'overlay' or 'nearest neighbour approaches'.

Apart from the selection of an appropriate coefficient, the most important issue for reliable colocalization analysis concerns the decision between true or random, significant or nonsignificant colocalization. Colocalization coefficients cannot stand alone, but have to be analysed in the context of probability: high coefficients can be the product of enhanced signal densities inside a given ROI, whereas lower coefficients can point out colocalizing events with a high statistical significance. To address this issue, different approaches have been suggested in the past: (1) the use of adjacent channel frames (Lachmanovich *et al.*, 2003), (2) PC-cross correlation analysis or dual channel cross-correlation analysis (Barbarese *et al.*, 1995; van Steensel *et al.*, 1996), (3) consecutive

block scrambling within one channel (Costes *et al.*, 2004) or parallel block scrambling in the case of ICCS (Comeau *et al.*, 2008). The first approach is valid providing that adjacent frames with similar signal patterns exist, which is not the case in most experiments. The second approach leads to random scenarios without compromising the original fluorescence pattern. Surprisingly, it has only been discussed as a qualitative measure thus far. Also, the approach has been limited to direct cross-correlation or PC values; the potential to generate a solid statistical criteria has not been described until today.

We introduce radial displacements in the *xy*-plane and calculate $M1/2_{\mathrm{ROI}}$ values along the distances (Eqs. 2–4). As we show in Figs. 3 and 4, the CDA generates channel-specific random regimes that can be used to calculate PDFs and lead to solid statistical criteria for true and random colocalization in terms of p values. On the other hand, PDFs for block scrambling depend on the size of the blocks. In general, cuts between adjacent pixels lead to artificially high-randomization scenarios. Spatial correlations between adjacent pixel intensities exist in response to the subjacent signal distribution and the convolution with the respective PSFs. A block size of 200 nm (similar to FWHM blocks; Costes *et al.*, 2004) interferes severely with the spatial interdependence between adjacent pixels (Figs. 3a and S3). Even for a block size of 360 nm, the randomized scenario provides visual and statistical evidence that the original structure is compromised: for 9×9 blocks still $\sim$40% of the pixels lose connectivity with at least one of their neighbours. By contrast, CDA generates random scenarios but maintains the spatial correlations of signal pattern. In our example, 2σ values for CDA are significantly higher than 2σ values for block scrambling, which indicate over-randomization thereby challenging previously published results of significant colocalization. False-positive true colocalization decisions are possible when PDFs do not represent a realistic random scenario. However, block scrambling can represent a random scenario reliably, when the block size is chosen adequately and the circumference of the block becomes small in respect to the block area. In addition, block scrambling can have advantages for the randomization of images with periodic fluorescence pattern.

It should be emphasized that the CDA in combination with $M1/2_{\mathrm{ROI}}$ generate channel-specific random scenarios, taking into account the respective signal densities. In consequence, the initial $M1/2_{\mathrm{ROI}}$ values at $d = 0$ can be tested independently in terms of p values. In the past, the significance of calculated Manders coefficients has been tested with PDFs that were derived from PCs (Costes *et al.*, 2004). However, Manders coefficients and PC follow different mathematical approaches, and randomization of pixel intensities can alter $M1/2_{\mathrm{ROI}}$ values and PCs to different degrees. Our approach allows classifying true and random colocalization for $M1/2_{\mathrm{ROI}}$ based on channel-specific random scenarios.

CDA confined to cellular compartments

Colocalization analysis based on $M1/2_{\mathrm{ICCS}}$ at the leading edge of migrating cells in combination with block scrambling and 'mean-padding' in user-defined ROIs has been reported recently (Comeau *et al.*, 2006). We see no problem at all in defining connected regions inside image frames before applying further image-processing routines. So far, dendrites and small subcellular compartments have been reported to be inaccessible for colocalization analysis (Comeau *et al.*, 2008). As we demonstrate, reliable detection of true against random colocalization can be achieved when CDA is performed inside confined compartments (Fig. 5). Obviously, the specific morphology of a cellular compartment is just as important as the segmentation of the fluorescence signals itself.

Driven by the task to access colocalization of $GABA_BR1/R2$ inside the core region and the PM separately, we applied CDA to PM with and without confinement. The morphology of the PM and the core region was determined carefully with transfected neurons (Fig. 5b). Our algorithm fits the complex dendrite morphology and dissects the first layer of receptor signals near the PM. Without confinement, CDA leads to a statistically significant colocalization even for scenarios with 0% colocalization; signals are simply shifted away from each other and the coefficients drop to zero. By contrast, confinement to the PM or to the core region guarantees constant signal densities and maintains pixel vicinities in the best possible way; structure-sensitive random scenarios can be created (see example movies in 'Supporting Information' and Fig. 3a, VI). Obviously, there is a limit for compartments with very complex border morphology or diameters that are smaller than the FWHM values of the subjacent PSFs. It should be emphasized that green and red point sources are affected differently by wavelength-dependent PSFs (Fig. 2). After convolution, red signals are broader than green signals and segmentation leads to slightly different ROIs. Manders coefficients calculated for 100% colocalization yield $M1_{\mathrm{ROI}} = 0.986$ (Fig. 3b) and $M2_{\mathrm{ROI}} = 0.934$ (not shown). In biological samples, $M1/2_{\mathrm{ROI}}$ values for 100% colocalization depend on the specificity of the antibodies, the fluorescent probes, the microscopic settings and the segmentation procedure. As Fig. 5b shows, a Manders coefficient of $\sim$0.75 can already be regarded as high. Although maximum values for Manders coefficients are difficult to estimate, the values for the random scenarios of a given experimental condition can be calculated directly by the CDA. Random coefficients increase with increasing signal density inside a ROI. In addition, 2σ values of the PDFs depend on the morphology and the topology of the given fluorescence pattern: 2σ values are small for randomly distributed small signals, whereas they increase with larger or connected signals and periodic pattern. For a given experiment, the similarity of the obtained PDFs to Gauss distributions should be tested by fitting algorithms to decide if p-value statistics for significance can be applied.

Colocalization of $GABA_BR$ subunits at the PM of hippocampal neurons

The formation of functional $GABA_BRs$ at the neuronal PM requires the assembly and heteromerization of $GABA_BR1/R2$. The existence of cell surface heteromers has been demonstrated earlier by biochemical, functional and microscopic analyses (Bettler *et al.*, 2004). Our results utilizing the CDA for PM signals show a high and significant colocalization of $GABA_BR1/R2$ at the cell surface in agreement with these observations. More importantly, by providing information from previously inaccessible compartments, such as the intracellular domains of dendrites and axons, CDA surprisingly revealed that $GABA_BR$ subunits are segregated in trafficking organelles distal from the cell body (Ramirez *et al.*, 2009). Our observations combine conventional trafficking with the analysis of the topology of secretory organelles and suggest that $GABA_BR$ assembly occurs in the somatic and dendritic endoplasmic reticulum (ER) (Ramirez *et al.*, 2009). The results lead us to the prediction that subunit assembly, ER exit and insertion at the PM are rapid compared to the residency time of subunits in the ER. Findings like these contribute to reveal new regulatory mechanisms of the availability of neurotransmitter receptors in neurons: a central issue in synaptic neurobiology.

Final remarks and conclusions

We have introduced the CDA as a robust method to detect true and random colocalization for experimental scenarios, which have not been addressed before. The approach is not restricted to fluorescent wide field or confocal microscopy; it could also be applied with emerging techniques such as PALM, STED or SIM, which have recently opened the access to fluorescence patterns below the optical diffraction limit (Hell *et al.*, 2004; Betzig *et al.*, 2006; Schermelleh *et al.*, 2008). In this context, the need to determine true and random colocalization inside small subcellular compartments will increase in the future.

The detection limits for colocalization within the CDA can be derived directly from the 2σ values of the calculated PDFs. 2σ values account for 95.4% of the area below a Gauss curve, which implicates that 2σ values of 0.047 ($M1_{ROI}$) define a detection limit of ~5% for statistical significance. PDFs are derived for the explicit signal characteristics of a given experiment; the decision for true or random colocalization is taken in the best possible context.

In summary, CDA can be applied easily and opens new possibilities to determine true and random colocalization down to subcellular levels. The basic needs for a rigorous analysis are (1) good quality two-channel fluorescent images, (2) two binary images with channel-specific ROIs and (3) one binary image that define the ROI of a confined cellular compartment. Success or failure of this approach is limited by the quality of the biological data itself.

Software

We provide an ImageJ plugin and an interactive 'online version' for the calculation of CDA for a given image set with the possibility to download the $M1/2_{ROI}(d)$ and subjacent statistics on our web page for Scientific Image Analysis (www.scian.cl).

Acknowledgements

The authors thank D. Diaz-Espinoza and M. Osorio-Reich for the ImageJ plugin, N. Contreras from Area Kreativa for support with the figures and J. Cowan for insightful comments on the paper. SCIAN-Lab is a selected member of the German–Chilean Center of Excellence Initiative for Medical Informatics (DAAD). Research in SCIAN-Lab (SH) is funded by FONDECYT 1090246, FONDEF D07I1019 and PBCT ACT47 (CONICYT, Chile). A.G. is funded by D07I1019. O.R. is funded by FONDECYT 1090246. A.C. is funded by FONDECYT 1071001. S.H. and A.C. are members of NEMO, ICM-P04-068-F and the Advanced Imaging & Bioinformatics Initiative (AIBI) (www.aibi.cl).

References

Adler, J. & Parmryd, I. (2007) Recent review on colocalization seem to misunderstand the Pearson correlation coefficient. *J. Microsc.* **227**, 83; author reply 84–85.

Adler, J., Pagakis, S.N. & Parmryd, I. (2008) Replicate-based noise corrected correlation for accurate measurements of colocalization. *J. Microsc.* **230**, 121–133.

Bacia, K. & Schwille, P. (2007) Fluorescence correlation spectroscopy. *Methods Mol. Biol.* **398**, 73–84.

Banker, G. & Goslin, K. (1988) Developments in neuronal cell culture. *Nature* **336**, 185–186.

Barbarese, E., Koppel, D.E., Deutscher, M.P., Smith, C.L., Ainger, K., Morgan, F. & Carson, J.H. (1995) Protein translation components are colocalized in granules in oligodendrocytes. *J. Cell Sci.* **108**(Pt. 8), 2781–2790.

Berezovska, O., Ramdya, P., Skoch, J., Wolfe, M.S., Bacskai, B.J. & Hyman, B.T. (2003) Amyloid precursor protein associates with a nicastrin-dependent docking site on the presenilin 1-gamma-secretase complex in cells demonstrated by fluorescence lifetime imaging. *J. Neurosci.* **23**, 4560–4566.

Bettler, B., Kaupmann, K., Mosbacher, J. & Gassmann, M. (2004) Molecular structure and physiological functions of GABA(B) receptors. *Physiol. Rev.* **84**, 835–867.

Betzig, E., Patterson, G.H., Sougrat, R., Lindwasser, O.W., Olenych, S., Bonifacino, J.S., Davidson, M.W., Lippincott-Schwartz, J., *et al.* (2006) Imaging intracellular fluorescent proteins at nanometer resolution. *Science* **313**, 1642–1645.

Bolte, S. & Cordelieres, F.P. (2006) A guided tour into subcellular colocalization analysis in light microscopy. *J. Microsc.* **224**, 213–232.

Bolte, S.a.F.P.C. (2007) Reply to Letter to the Editor. *J. Microsc.* **227**, 1.

Box, G.E.P. & Muller, M.E. (1958) A note on the generation of random normal deviates. *Annals Math. Stat.* **29**, 610–611.

Brown, M.C. (2007) Fluorescence microscopy – avoiding the pitfalls. *J. Cell Sci.* **120**, 1703–1705.

Comeau, J.W., Costantino, S. & Wiseman, P.W. (2006) A guide to accurate fluorescence microscopy colocalization measurements. *Biophys. J.* **91**, 4611–4622.

Comeau, J.W., Kolin, D.L. & Wiseman, P.W. (2008) Accurate measurements of protein interactions in cells via improved spatial image cross-correlation spectroscopy. *Mol. Biosyst.* **4**, 672–685.

Costes, S.V., Daelemans, D., Cho, E.H., Dobbin, Z., Pavlakis, G. & Lockett, S. (2004) Automatic and quantitative measurement of protein-protein colocalization in live cells. *Biophys. J.* **86**, 3993–4003.

Couve, A., Filippov, A.K., Connolly, C.N., Bettler, B., Brown, D.A. & Moss, S.J. (1998) Intracellular retention of recombinant GABAB receptors. *J. Biol. Chem.* **273**, 26361–26367.

David, P.S., Tanveer, R. & Port, J.D. (2007) FRET-detectable interactions between the ARE binding proteins, HuR and p37AUF1. *RNA* **13**, 1453–1468.

Demandolx, D. & Davoust, J. (1997) Multicolour analysis and local image correlation in confocal microscopy. *J. Microsc.* **185**, 21–36.

Espinosa, A., Garcia, A., Hartel, S., Hidalgo, C. & Jaimovich, E. (2009) NADPH oxidase and hydrogen peroxide mediate insulin-induced calcium increase in skeletal muscle cells. *J. Biol. Chem.* **284**, 2568–2575.

Fanani, M.L., De Tullio, L., Härtel, S., Jara, J. & Maggio, B. (2009) SMase-induced domain growth and shape relaxation driven by a rate-dependent, out-of-equilibrium, compositional change. *Biophys. J.* **96**, 67–76.

Fink, C., Morgan, F. & Loew, L.M. (1998) Intracellular fluorescent probe concentrations by confocal microscopy. *Biophys. J.* **75**, 1648–1658.

Härtel, S., J. Jara, C.G. Lemus & Concha, M.L. (2007) 3D morpho-topological analysis of asymmetric neuronal morphogenesis in developing Zebrafish. *Computational Modelling of Objects Represented in Images*. Fundamentals, Methods and Applications (ed. by J.M. Tavares & J. Nata), pp. 6. Taylor and Francis, London.

Hell, S.W., Dyba, M. & Jakobs, S. (2004) Concepts for nanoscale resolution in fluorescence microscopy. *Curr. Opin. Neurobiol.* **14**, 599–609.

Koyama-Honda, I., Ritchie, K., Fujiwara, T., Iino, R., Murakoshi, H., Kasai, R.S. & Kusumi, A. (2005) Fluorescence imaging for monitoring the colocalization of two single molecules in living cells. *Biophys. J.* **88**, 2126–2136.

Lachmanovich, E., Shvartsman, D.E., Malka, Y., Botvin, C., Henis, Y.I. & Weiss, A.M. (2003) Co-localization analysis of complex formation among membrane proteins by computerized fluorescence microscopy: application to immunofluorescence co-patching studies. *J. Microsc.* **212**, 122–131.

Landmann, L. (2002) Deconvolution improves colocalization analysis of multiple fluorochromes in 3D confocal data sets more than filtering techniques. *J. Microsc.* **208**, 134–147.

Manders, E.M., Stap, J., Brakenhoff, G.J., van Driel, R. & Aten, J.A. (1992) Dynamics of three-dimensional replication patterns during the S-phase, analysed by double labelling of DNA and confocal microscopy. *J. Cell Sci.* **103**(Pt. 3), 857–862.

Manders, E.M., Verbeek, F.J. & Aten, A. (1993) Measurement of co-localization of objects in dual color confocal images. *J. Microsc.* **169**, 375–382.

Parra, V., Eisner, V., Chiong, M., Criollo, A., Moraga, F., Garcia, A., Härtel, S., Jaimovich, E., *et al.* (2008) Changes in mitochondrial dynamics during ceramide-induced cardiomyocyte early apoptosis. *Cardiovasc. Res.* **77**, 387–397.

Pearson, H. (2007) The good, the bad and the ugly. *Nature* **447**, 138–140.

Ramirez, O.A., Vidal, R.L., Tello, J.A., Vargas, K.J., Kindler, S., Hartel, S. & Couve, A. (2009) Dendritic assembly of heteromeric gamma-aminobutyric acid type B receptor subunits in hippocampal neurons. *J. Biol. Chem.* **284**, 13077–13085.

Sanchez, G., Escobar, M., Pedrozo, Z., Macho, P., Domenech, R., Hartel, S., Hidalgo, C. & Donoso, P. (2008) Exercise and tachycardia increase NADPH oxidase and ryanodine receptor-2 activity: possible role in cardioprotection. *Cardiovasc. Res.* **77**, 380–386.

Savio-Galimberti, E., Frank, J., Inoue, M., Goldhaber, J.I., Cannell, M.B., Bridge, J.H. & Sachse, F.B. (2008) Novel features of the rabbit transverse tubular system revealed by quantitative analysis of three-dimensional reconstructions from confocal images. *Biophys. J.* **95**, 2053–2062.

Schermelleh, L., Carlton, P.M., Haase, S., Shao, L., Winoto, L., Kner, P., Burke, B., Cardoso, M.C., *et al.* (2008) Subdiffraction multicolor imaging of the nuclear periphery with 3D structured illumination microscopy. *Science* **320**, 1332–1336.

Scriven, D.R., Lynch, R.M. & Moore, E.D. (2008) Image acquisition for colocalization using optical microscopy. *Am. J. Physiol. Cell Physiol.* **294**, C1119–1122.

van Steensel, B., van Binnendijk, E.P., Hornsby, C.D., van der Voort, H.T., Krozowski, Z.S., de Kloet, E.R. & van Driel, R. (1996) Partial colocalization of glucocorticoid and mineralocorticoid receptors in discrete compartments in nuclei of rat hippocampus neurons. *J. Cell Sci.* **109**(Pt. 4), 787–792.

Vidal, R.L., Ramirez, O.A., Sandoval, L., Koenig-Robert, R., Hartel, S. & Couve, A. (2007) Marlin-1 and conventional kinesin link GABAB receptors to the cytoskeleton and regulate receptor transport. *Mol. Cell Neurosci.* **35**, 501–512.

Supporting Information

Additional Supporting Information may be found in the online version of this article:

Fig. S1. Automated segmentation fails for $GABA_BR1$ signals inside hippocampal neurons and for point signals in model dendrites.
Fig. S2. PDFs of PC and $M1_{ROI}$ for block 5, block 9, and CDA.
Fig. S3. Effect of block scrambling on size and morphology of segmented point signals.
Movie S1. CDA for 100% colocalizing point sources in model dendrite.
Movie S2. CDA of $GABA_BR1/R2$ in hippocampal dendrite.
Movie S3. CDA of $GABA_BR1/2$ in core region of hippocampal dendrite.
Movie S4. CDA of $GABA_BR1/2$ in region near the plasma membrane of a hippocampal dendrite.

Please note: Wiley-Blackwell are not responsible for the content or functionality of any supporting materials supplied by the authors. Any queries (other than missing material) should be directed to the corresponding author for the article.